RSC Advances

PAPER

View Article Online
View Journal | View Issue

Cite this: *RSC Adv.*, 2020, **10**, 1956

Synthesis of a furfural-based DOPO-containing co-curing agent for fire-safe epoxy resins†

Weiqi Xie, ‡[a] Shiwen Huang,‡[a] Donglin Tang, [a] Shumei Liu *[ab] and Jianqing Zhao*[ab]

Received 16th August 2019
Accepted 7th December 2019

DOI: 10.1039/c9ra06425g

rsc.li/rsc-advances

A furfural-based DOPO-containing flame retardant, 6,6′-(((methylenebis(4,1-phenylene))bis(azanediyl)) bis(furan-2-ylmethylene))bis(dibenzo[*c*,*e*][1,2]oxaphosphinine 6-oxide) (MBF-DOPO), was synthesized and utilized as a co-curing agent of 4,4′-diaminodiphenyl methane (DDM) for fire-safe epoxy thermosets. For the cured epoxy resin containing 4.0% MBF-DOPO, the limiting oxygen index (LOI) reached 32.9% (with the V-0 rating in UL-94 test), and the peak heat release rate and total smoke production values were respectively decreased by 29.3% and 33.6%, compared to pure epoxy resin. Scanning electron microscopy (SEM) and Fourier transform infrared spectroscopy (FTIR) results confirmed that the furfural-based flame retardant MBF-DOPO promoted the charring formation of the epoxy matrix, which effectively isolated the gas and heat transfer during combustion and thus enhanced the fire-safety performance of the epoxy thermosets. This work provides an effective route for synthesizing a furfural-based flame retardant, which possesses great potential for application in fire-safe epoxy thermosets.

Introduction

Recently, there has been more and more interest in the preparation of new materials and chemicals from furfural, which is a multi-functional compound containing a furan ring and an aldehyde group.[1,2] It is mainly extracted from abundant agricultural residues like plant hulls and corn cobs, thus enabling furfural to be more feasible as a platform molecule for renewable chemicals and materials.[3,4] Moreover, with a reactive aldehyde group, furfural is deemed to be a promising renewable resource for preparing various chemicals and materials, and has been used in diverse research fields.[5,6]

Epoxy resins are a significant class of polymers and have been adopted in many different fields (*i.e.*, coatings, adhesive, and laminate materials) for their excellent chemical resistance and mechanical properties.[7–10] However, epoxy resins have the drawback of poor fire resistance performance, which greatly limits their application in areas requiring high flame retardancy.[11] Various kinds of flame retardants (phosphorus-, nitrogen- and silicon-containing compounds) were adopted to improve the fire-safety performance of epoxy resins.[12–14] Among them, 9,10-dihydro-9-oxa-10-phosphaphenanthrene-10-oxide (DOPO) and its derivatives are eco-friendly flame retardants with many advantages (*e.g.*, high efficiency and low toxicity).[15,16] Recently, the preparation of a furfural-based flame retardant has aroused extensive attention for sustainable development.[17–19] In order to meet the urgent needs for achieving sustainable development, the preparation of DOPO derivatives derived from furfural is a potential and sustainable strategy.[20] However, the preparation of furfural-based DOPO derivatives for epoxy resins is still in its infancy.

Herein, a novel furfural-based DOPO derivative, 6,6′-(((methylenebis(4,1-phenylene))bis(azanediyl))bis(furan-2-ylmethylene))bis(dibenzo[*c*,*e*][1,2]oxaphosphinine 6-oxide) (MBF-DOPO), is prepared and utilized as a co-curing agent of 4,4′-diaminodiphenyl methane (DDM) for fire-safe epoxy thermosets. It is expected that the flame retardancy from furfural and DOPO will have outstanding fire resistance efficiency. Moreover, the thermal and mechanical performance of epoxy thermosets are also evaluated.

Materials and methods

Materials

4,4′-Diaminodiphenyl methane (DDM), DOPO, and furfural were obtained from Aladdin Reagent Co. Ltd., China. DGEBA (epoxy value = 0.51 mol/100 g) was obtained from SINOPEC Baling company, China. 1,4-Dioxane and ethanol were obtained from Guangzhou Chemical Reagent Factory, China.

[a]*School of Materials Science and Engineering, South China University of Technology, Guangzhou, 510640, P. R. China. E-mail: liusm@scut.edu.cn; psjqzhao@scut.edu.cn; Fax: +86-13611400566; +86-13609724000; Tel: +86-13611400566; +86-13609724000*

[b]*Key Laboratory of Polymer Processing Engineering, Ministry of Education, Guangzhou 510640, P. R. China*

† Electronic supplementary information (ESI) available. See DOI: 10.1039/c9ra06425g

‡ These authors contributed equally to this work.

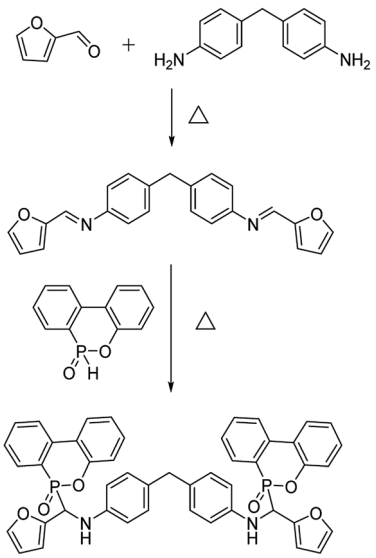

Fig. 1 Synthesis route of MBF-DOPO.

Synthesis of MBF-DOPO

DDM (9.91 g, 0.05 mol) and furfural (9.61 g, 0.10 mol) were added to 200 mL of 1,4-dioxane under a N_2 atmosphere. After continuous stirring for 3 h at 80 °C, the system was cooled to room temperature, followed by the addition of 100 mL of 1,4-dioxane solution containing DOPO (21.6 g, 0.10 mol) into the system and then stirred at 55 °C for 12 h. After that, the mixture was transferred to ice water. The crude product was filtered, washed (three times using ethanol) and vacuum dried (75 °C for 24 h) to give a white powder (the yield was 92.4%). The synthetic route of MBF-DOPO is depicted in Fig. 1.

Preparation of epoxy networks

The epoxy networks were prepared by the curing reaction of DGEBA with various weights of DDM and MBF-DOPO (see Table 1, the molar ratio of the N–H in DDM and MBF-DOPO to epoxy groups is 1). DGEBA and MBF-DOPO were added to a flask and stirred at 170 °C for 60 min. After that, the system was cooled to 80 °C, followed by adding DDM. The mixture was stirred for 20 min, and poured into a mould and degassed at 80 °C for 20 min. Afterward, the reaction system was cured at 80 °C for 2 h, 110 °C for 2 h, and 180 °C for 2 h to obtain the epoxy networks. The preparation route for epoxy network is depicted in Fig. 2.

Characterization

^1H, ^{13}C and ^{31}P nuclear magnetic resonance (NMR) spectra were collected with a Bruker NMR spectrometer (Billerica, MA, USA) and deuterated dimethylsulfoxide (DMSO-d6) was used as the solvent. The infrared spectra (FT-IR) were obtained with a Vertex70 spectrometer (Bruker, Billerica, MA, USA) using KBr pellets. Mass spectrometry (MS) spectra were collected on a maXis impact mass spectrometer (Bruker).

Thermogravimetric analyses (TGA) were conducted using a TG-209F1 TGA (Netzsch, Selb, Germany) at a heating rate of 10 °C min^{-1} (N_2 atmosphere), and the temperature range is from 50 to 700 °C. Dynamic mechanical analysis (DMA) was conducted using a TA instrument (DMA Q800, America) at a heating rate of 3 °C min^{-1} (from 25 to 230 °C). The dimensions of the cured samples for measurement were 40 × 10 × 3.0 mm.

Tensile and flexural properties were analyzed based on ASTM D638-08 and ASTM D790-07, respectively, on an Instron-5967 universal electronic testing machine.

UL-94 vertical burning tests were conducted with a UL 94 flame chamber (Fire Testing Technology, UK) according to ASTM D3801-10 (sample dimension of 125 × 13 × 3 mm). Limiting oxygen index (LOI) tests were conducted using an oxygen index instrument (Fire Testing Technology, UK) according to ASTM D2863-97 (sample dimension of 150 × 6.5 × 3.2 mm). Cone calorimeter tests (CCT) were conducted using a FTT cone calorimeter according to ISO5660 (sample dimension of 100 × 100 × 5 mm).

Scanning electron microscopy (SEM) experiments were conducted with a NOVA NANOSEM 430 machine. The sample was sputter-coated with gold before testing. X-ray photoelectron spectroscopy (XPS) was conducted using an Axis Ultra spectrometer (Kratos, England). Raman spectroscopy was conducted using a DXR laser Raman spectrometer (532 nm Helium–Neon line) at room temperature. Thermogravimetry-Fourier transform infrared spectroscopy (TGA-FTIR) tests were conducted with a STA449C/3MFC/G instrument (Bruker, USA) (N_2 atmosphere, heating rate = 20 °C min^{-1}).

Table 1 Stoichiometric formulation of the epoxy system

Samples[a]	DGEBA (wt%)	DDM (wt%)	MBF-DOPO (wt%)	DOPO (wt%)	P (wt%)
EP-0	79.83	20.17	0	0	0
EP-1.0	79.03	19.97	1.0	0	0.08
EP-2.0	78.23	19.77	2.0	0	0.16
EP-3.0	77.44	19.56	3.0	0	0.24
EP-4.0	76.64	19.36	4.0	0	0.31
EP-DOPO-4.0	76.64	19.36	0	4.0	0.57
EP-5.0	75.84	19.16	5.0	0	0.39

[a] Sample name: EP-X, *X* represents the weight percentage of MBF-DOPO in the MBF-DOPO/DDM/DGEBA system. EP-DOPO-4.0 represents 4 wt% DOPO in the DOPO/DDM/DGEBA system.

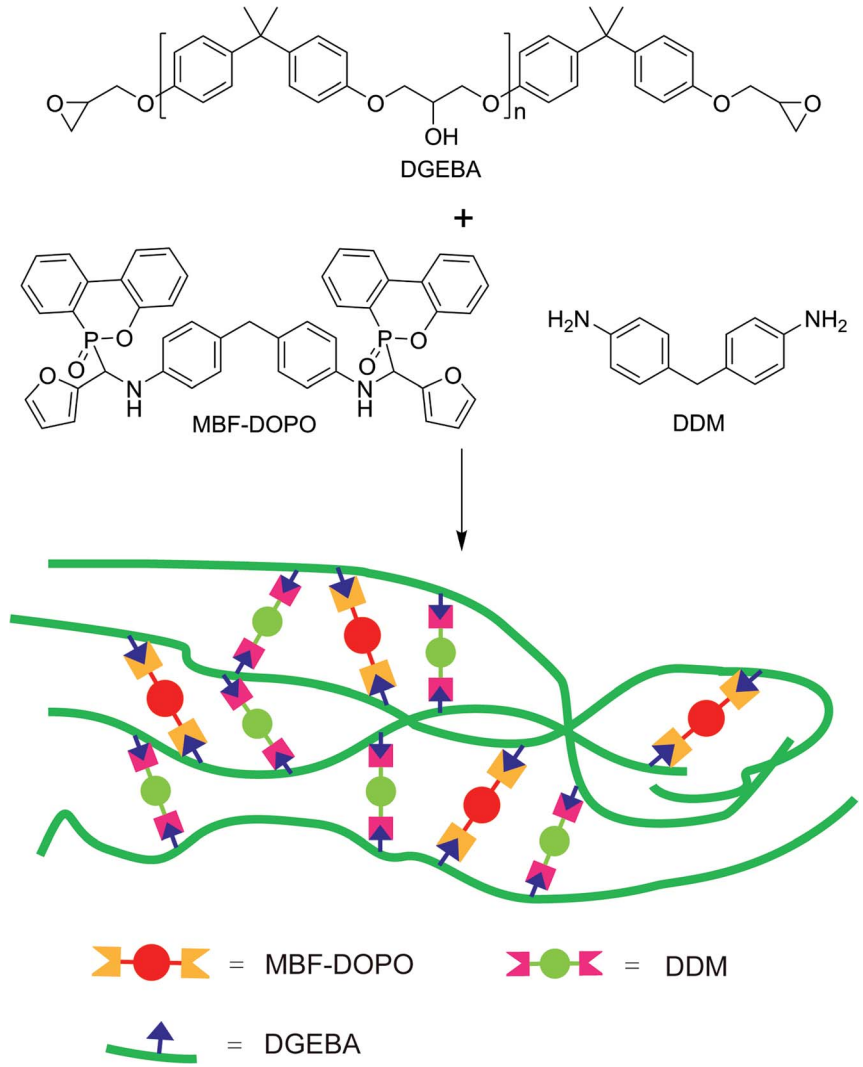

Fig. 2 Route for preparation of the cured network MBF-DOPO/DDM/DGEBA.

Results and discussion

Characterization of MBF-DOPO

The structure of the obtained MBF-DOPO was characterized by FT-IR, NMR, and MS techniques. The FTIR spectra of furfural, DDM, DOPO and MBF-DOPO are shown in Fig. S1.† In the FTIR spectrum of MBF-DOPO, a few peaks disappeared compared with the spectra of furfural, DDM and DOPO, such as the peak at 3430 cm^{-1} (primary amine (N–H) stretching) in the DDM spectrum, the peak at 2430 cm^{-1} (P–H stretching) in the DOPO spectrum and the peak at 1675 cm^{-1} (C=O stretching) in the furfural spectrum. Meanwhile, a peak corresponding to the secondary amine (C–NH) stretching appears at 3320 cm^{-1} in the MBF-DOPO spectrum. The above results confirm the successful synthesis of MBF-DOPO.

The ^{1}H NMR spectra of furfural, DDM, DOPO, and MBF-DOPO are shown in Fig. 3(a). The characteristic proton of N–CH (δ = 5.19 ppm) is found in the MBF-DOPO spectrum, following the disappearance of the peak of P–H (δ = 8.64 ppm) in the DOPO spectrum, the peak of CH=O (δ = 9.62 ppm) in the furfural spectrum and the peak of the primary amine (N–H, δ = 4.79 ppm) in the DDM spectrum. Fig. S2† illustrates the assignment of peaks in the ^{1}H-NMR spectrum of MBF-DOPO, ^{1}H NMR (DMSO-d_6, ppm): δ = 2.50 (DMSO), 3.33 (H_2O), 3.47 (H_{16}), 5.19 (H_{12}), 6.11 (H_{11}), 6.37 (H_{10}), 6.43–6.74 (H_{14}, H_{15}, H_{17}, H_{18}), 7.07–7.82 (H_{1-3}, H_{6-9}), 7.94 (H_5), and 8.16–8.19 (H_4, H_{13}). The structure of MBF-DOPO is also confirmed by ^{13}C and ^{31}P NMR and MS spectra (Fig. 3(b)–(d)). In Fig. 3(b), the expected chemical shifts of the C atoms are in good agreement with the actual chemical shifts, ^{13}C NMR (DMSO-d_6, ppm): δ = 51.2 (C_9), 66.8 (C_{24}), 109.8 (C_{22}), 111.2 (C_{21}), 114.1 (C_4, C_6), 120.4–120.6 (C_2, C_8), 121.9 (C_{11}), 122.8 (C_{14}), 123.8–126.0 (C_{12}, C_{15}, C_{19}), 128.9–129.1 (C_{10}, C_{17}), 130.8–132.1 (C_3, C_7), 134.0–134.3 (C_{16}, C_{18}), 135.9 (C_{13}), 143.5 (C_{20}), 145.2 (C_5), and 149.1–149.5 (C_1, C_{23}). The ^{31}P NMR spectrum of MBF-DOPO shows two peaks at 27.4 and 29.3 ppm, which are due to the chiral structure of the P atoms in MBF-DOPO.[21] The mass spectrometry (MS) spectrum shows an [M + Na^+] ion peak at m/z 809.1944, suggesting

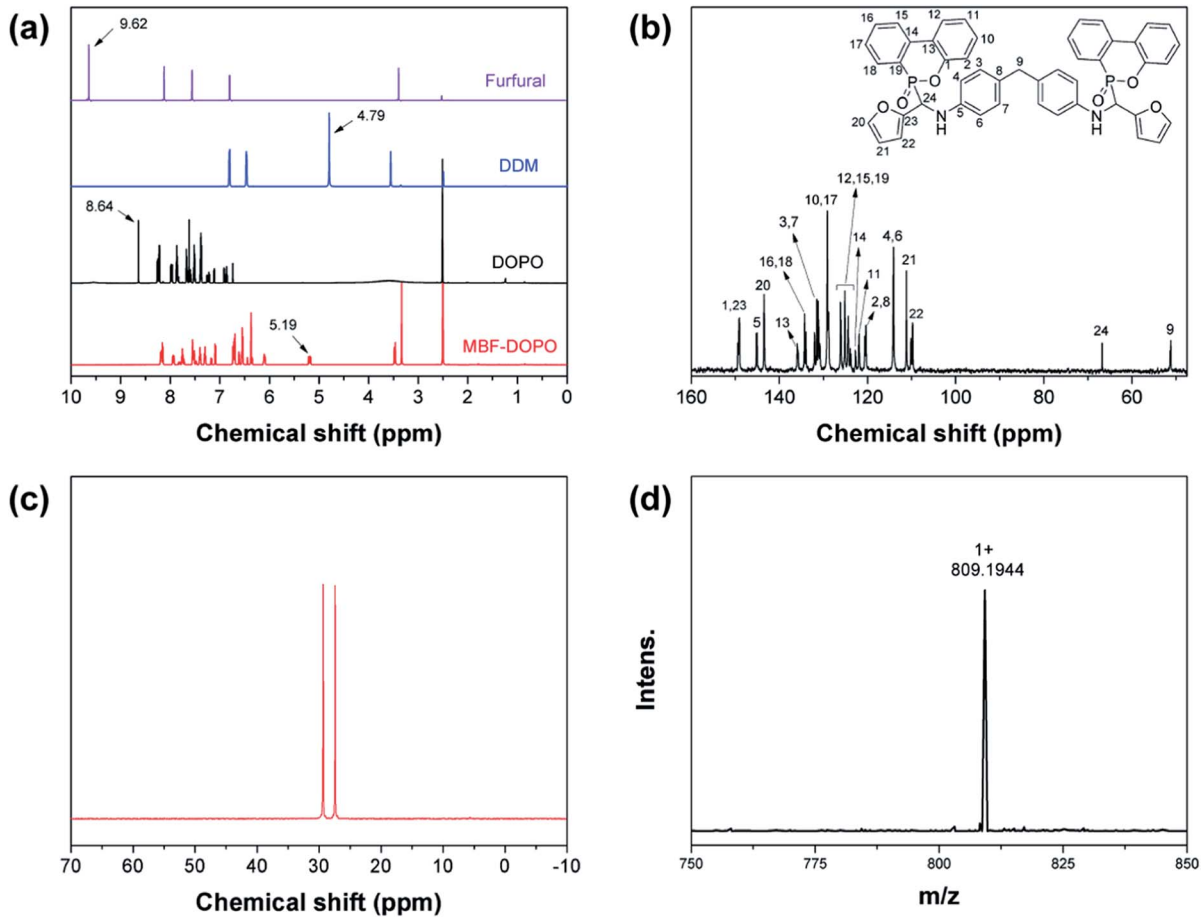

Fig. 3 (a) ^{1}H NMR spectra of furfural, DDM, DOPO, and MBF-DOPO. (b) ^{13}C-NMR, (c) ^{31}P-NMR, and (d) HRESI-MS spectra of MBF-DOPO.

a molecular formula of $C_{47}H_{36}N_2O_6P_2$. All these results fully confirm the successful synthesis of MBF-DOPO with a facile and environmental-friendly route. The TGA curves of MBF-DOPO and DOPO (N_2 and air atmosphere) are shown in Fig. 4. As seen from Fig. 4(a), DOPO possesses an initial decomposition temperature ($T_{5\%}$) of 217.7 °C under a N_2 atmosphere, whereas MBF-DOPO exhibits a $T_{5\%}$ of 312.0 °C, suggesting that MBF-DOPO possesses a higher thermal stability compared with DOPO. The residue (at 700 °C) of MBF-DOPO is 38.9% under a N_2 atmosphere, which is far higher than DOPO (1.73%). Similarly, in air atmosphere (Fig. 4(b)), MBF-DOPO shows a higher $T_{5\%}$ (336.7 °C) and residue (at 700 °C, 41.8%) compared

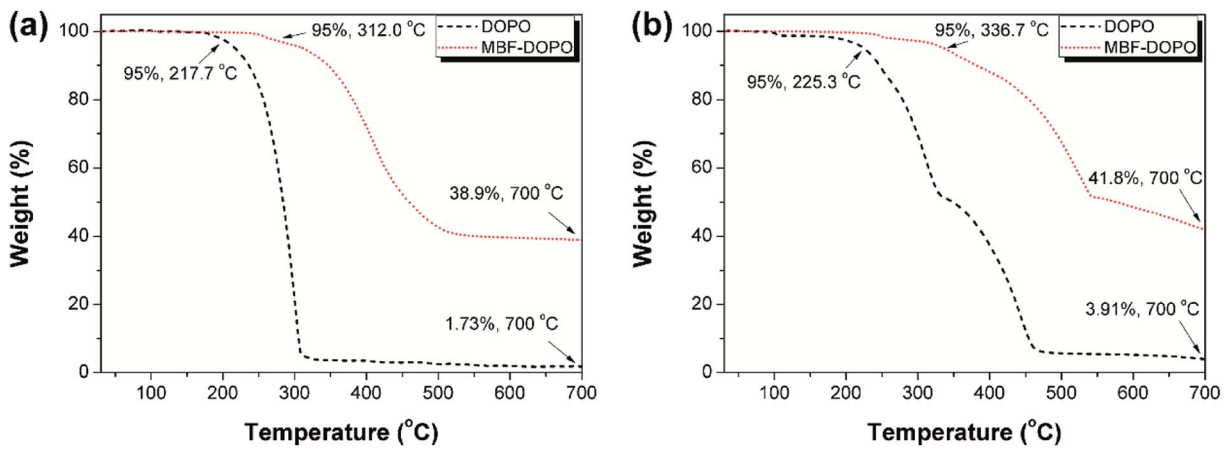

Fig. 4 TGA curves of MBF-DOPO and DOPO under a (a) N_2 and (b) air atmosphere.

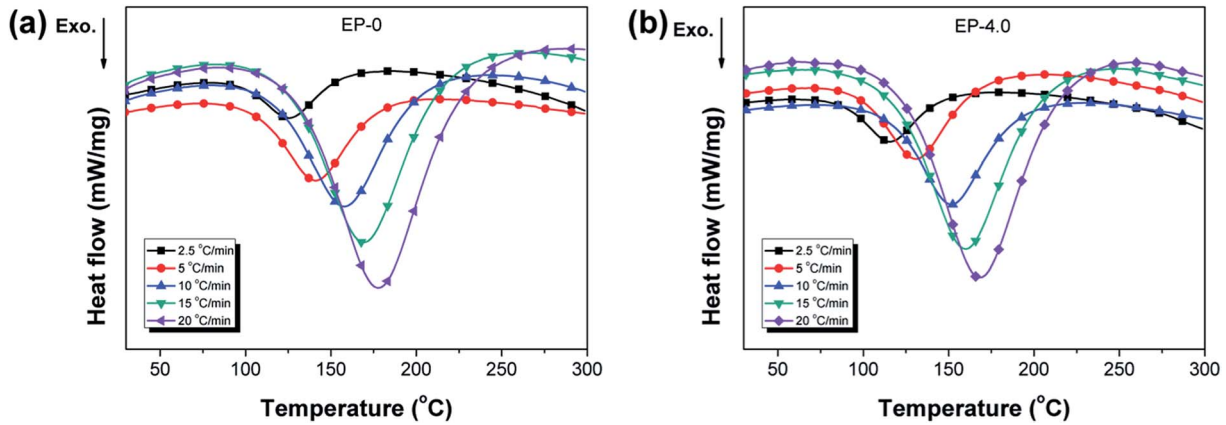

Fig. 5 DSC thermograms of (a) EP-0 and (b) EP-4.0 cured at varying heating rates.

with DOPO. The TGA results indicate that the furfural-based compound MBF-DOPO possesses excellent charring ability associated with high thermal stability, which is mainly caused by the thermally-stable benzene and furan ring structures in MBF-DOPO.

Curing behavior of the MBF-DOPO/DDM/DGEBA system

In the MBF-DOPO/DDM/DGEBA system, the main reaction for the curing process is the ring opening of the epoxy by a reaction with the amine groups (primary or secondary amine) of DDM and MBF-DOPO.[21] The nonisothermal curing kinetics of the MBF-DOPO/DDM/DGEBA system are studied using DSC at various heating rates (2.5, 5, 10, 15 and 20 °C min^{-1}) and are depicted in Fig. 5. Kissinger's method is utilized for the calculation of the apparent activation energy,[22]

$$\ln\left(\frac{\beta}{T_p^2}\right) = \ln\left(\frac{AR}{E_a}\right) - \frac{E_a}{RT_p} \quad (1)$$

where β, R, and T_p respectively represent the heating rate, the ideal gas constant, and the exothermic peak temperature. E_a and A represent the apparent activation energy and the pre-exponential factor, respectively. Table S1† lists the T_p values of the EP-0 and EP-4.0 systems cured at various heating rates. According to eqn (1), the curing activation energy (E_a) of EP-0 and EP-4.0 is obtained from the linear plot of $\ln(\beta/T_p^2)$ *versus* $1/T_p$ plot (Fig. 6), as listed in Table S2.† It can be found that the EP-4.0 curing system possesses a lower E_a (47.3 kJ mol^{-1}) than the EP-0 curing system (50.4 kJ mol^{-1}), indicating that the introduction of MBF-DOPO in epoxy resins can lower the activation energy of the system and accelerate the crosslinking reaction.

Fire-safety performance

The fire-safety performance of cured resins is assessed by LOI and UL-94 vertical burning (UL-94) tests (see Table 2). The pure epoxy resin EP-0 possesses the LOI value of 23.5% with melt-dripping and no rating in the UL-94 test, and the LOI value increases with the increase of the MBF-DOPO content in the epoxy matrix. By adding 4.0 wt% of DOPO to the epoxy resin, EP-DOPO-4.0 shows a LOI value of 31.4% and passes the UL-94 V-1 rating. Compared with EP-DOPO-4.0, EP-4.0 (containing 4.0 wt% of MBF-DOPO) shows better fire-safety properties with a V-0 rating of the UL-94 test and increases its LOI value to 32.9%. The results show that MBF-DOPO possesses a higher flame-retardant efficiency for epoxy resins compared with DOPO. It may be deduced that the unique combination of phosphorus and nitrogen atoms in MBF-DOPO plays an important role in enhancing the flame-retardant efficiency of MBF-DOPO, and the synergistic effect between the phosphorus and nitrogen elements endows MBF-DOPO with a high flame-retardant performance in both the gas phase and condensed phase.

The fire-safety performance of EP-0 and EP-4.0 is further evaluated using the cone calorimeter test (CCT) (Fig. 7 and Table S3†). As can be seen, the time to ignition (TTI) value of EP-4.0 is lower than EP-0, which is due to the early decomposition of unstable phosphorus-containing structures from MBF-DOPO. The peak of the heat release rate (pHRR) of EP-4.0 is decreased to 680 kW m^{-2}, which is 29.3% lower than that of EP-0 (962 kW m^{-2}). Similarly, EP-4.0 possesses a 12.6% reduction in the total heat release (THR) value compared to EP-0. The

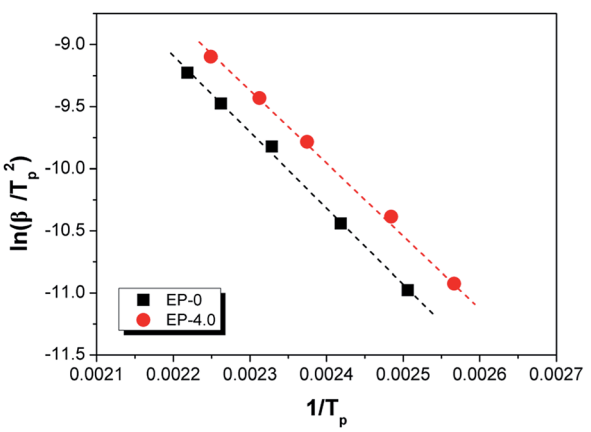

Fig. 6 Plot of $\ln(\beta/T_p^2)$ *versus* $1/T_p$ of EP-0 and EP-4.0 according to Kissinger's method.

Table 2 UL-94 vertical burning and LOI test result of cured MBF-DOPO/DDM/DGEBA

Samples	P (wt%)	LOI (%)	UL-94		
			$t_1 + t_2$ (s)	Dripping	Rating
EP-0	0	23.5 ± 0.3	Lasting burning	Yes	NR
EP-1.0	0.08	26.2 ± 0.2	78.5 ± 3.1	No	V-2
EP-2.0	0.16	28.3 ± 0.3	35.6 ± 1.7	No	V-1
EP-3.0	0.24	31.2 ± 0.3	19.5 ± 3.4	No	V-1
EP-4.0	0.31	32.9 ± 0.2	7.5 ± 2.1	No	V-0
EP-DOPO-4.0	0.57	31.4 ± 0.4	28.6 ± 4.7	No	V-1
EP-5.0	0.39	33.5 ± 0.3	5.2 ± 1.2	No	V-0

above results further verify the good fire resistance performance of MBF-DOPO for the epoxy matrix. As can be seen in Fig. 7(c), the residual mass of EP-4.0 after the cone calorimeter test is 17.9 wt%, and is far higher than that of EP-0 (8.6 wt%), which suggests that the introduction of MBF-DOPO may promote the char forming during combustion. The smoke production from combustion is a very significant indicator for the fire-safety properties of epoxy resins. In Fig. 7(d), compared to EP-0, the total smoke production (TSP) value of EP-4.0 is significantly decreased by 33.6%, suggesting that the introduction of MBF-DOPO helps to form compact and protective char layers, which act as protective barriers to suppress the smoke production of the epoxy matrix during combustion.

TG-FTIR analysis

TG-FTIR is utilized to understand the gas-phase flame-retardant effect of MBF-DOPO for epoxy resins by detecting the gases released from the thermal decomposition of EP-0 and EP-4.0. The FTIR spectra of gases obtained from the thermal decomposition of EP-0 and EP-4.0 at the initial degradation temperature (370 °C for EP-4.0, 390 °C for EP-0) and the maximum degradation temperature (390 °C for EP-4.0, 405 °C for EP-0) are

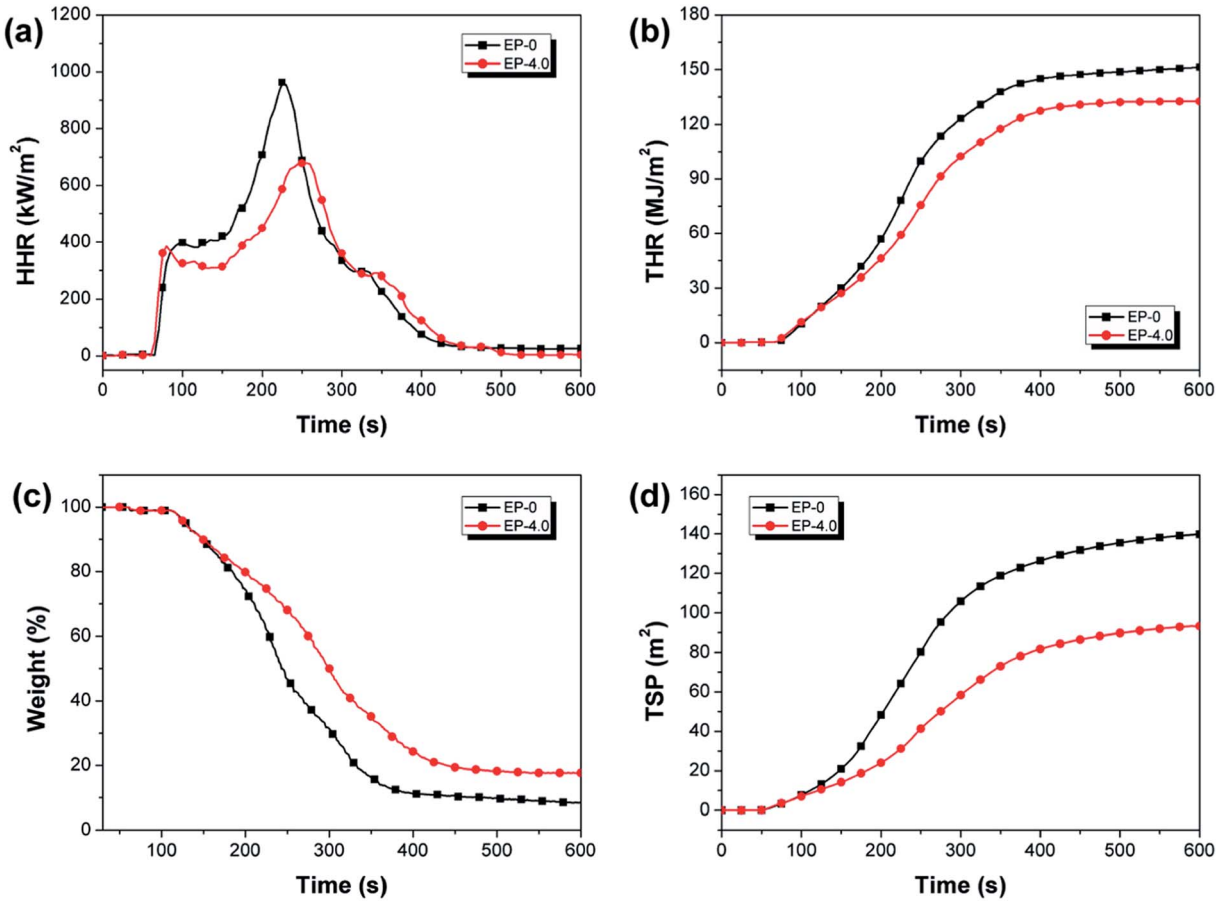

Fig. 7 (a) HRR, (b) THR, (c) residual mass, and (d) TSP curves of EP-0 and EP-4.0.

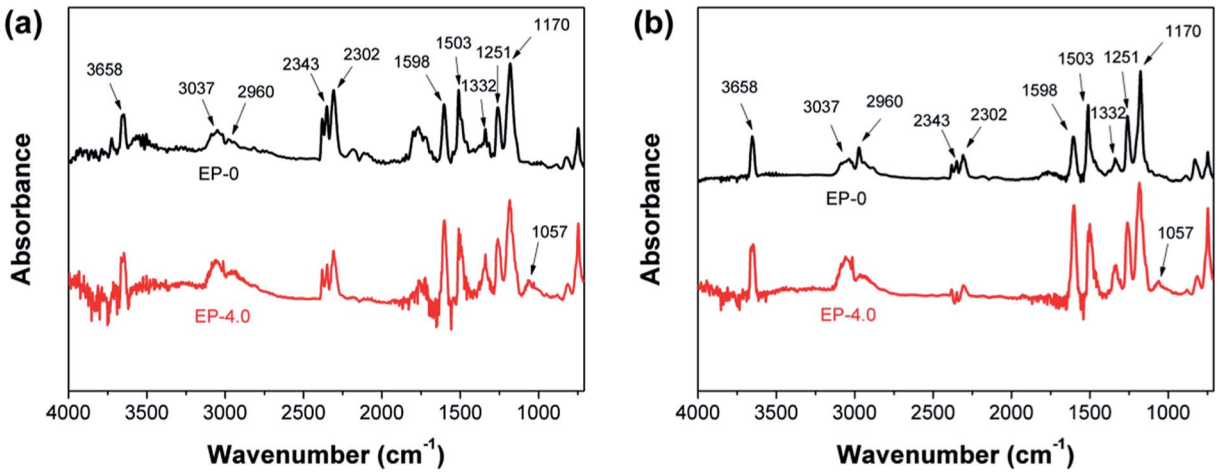

Fig. 8 FTIR spectra of the pyrolysis products of EP-0 and EP-4.0 at (a) the initial and (b) maximum degradation temperatures.

presented in Fig. 8. As can be seen, the gaseous products of EP-4.0 and EP-0 are identified by the absorptions at 1170 and 1251 cm^{-1} (ethers), 1598, 1503 and 1332 cm^{-1} (aromatic substances), 2343 and 2302 cm^{-1} (CO_2), 3037 and 2960 cm^{-1} (hydrocarbons), and 3658 cm^{-1} (phenols).[23,24] However, unlike EP-0, there is a new peak in the spectrum of EP-4.0, belonging to P–O–P (1057 cm^{-1}),[25] which is generated from the decomposition of MBF-DOPO in EP-4.0 during combustion, indicating that the phosphorus-containing gaseous products play an important role in the gas-phase flame-retardant effect of MBF-DOPO.

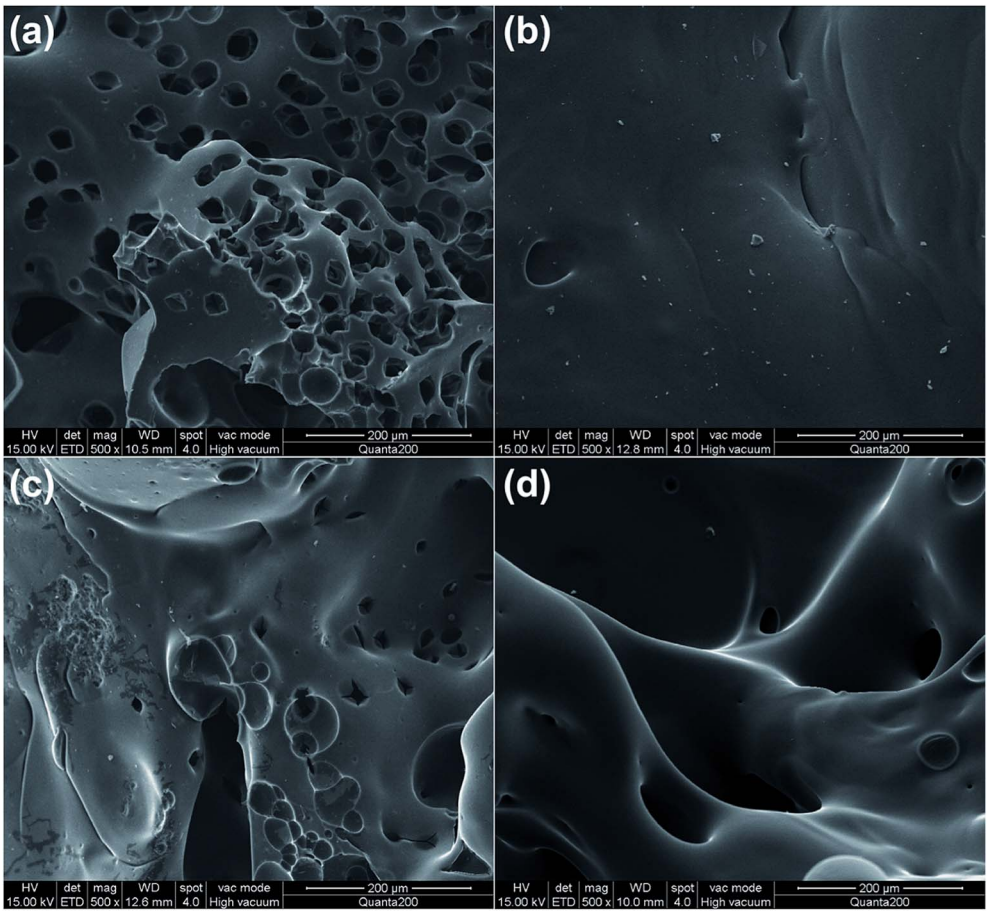

Fig. 9 SEM photographs of external ((a) EP-0, (b) EP-4.0) and internal char layers ((c) EP-0, (d) EP-4.0) after CCT.

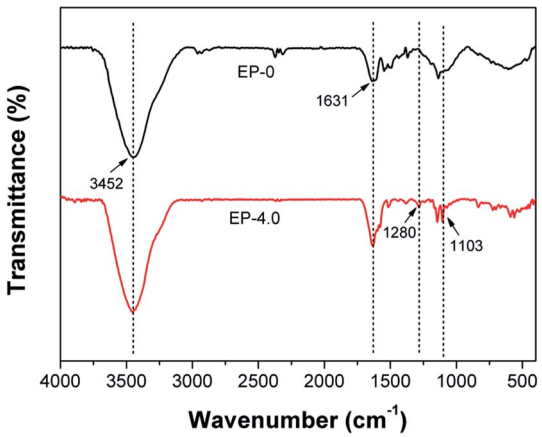

Fig. 10 FT-IR spectra of char residues after CCT.

Char analysis

The SEM morphology of the char residues after CCT is depicted in Fig. 9. For EP-0, both the external and internal char layers exhibit a cracked char residue with open holes. The external char layer of EP-4.0 presents a compact and homogeneous structure without broken bubbles, and the internal char layer shows a continuous and skeletal morphology with some small pores. The formation of the strong char layer in EP-4.0 inhibits the transmission of heat and gas during combustion, which endows EP-4.0 with excellent fire-safety performance.

The chemical structures of the char residue are measured with the FTIR technique. As shown in Fig. 10, both EP-0 and EP-4.0 have a peak at 3452 cm^{-1} (O–H or N–H stretching) and a peak at 1631 cm^{-1} (carbonized compound stretching). Compared with EP-0, two new characteristic peaks occur at 1103 cm^{-1} (P–O–C stretching) and 1280 cm^{-1} (P═O stretching) in the spectrum of EP-4.0, showing that the char residue of EP-4.0 contains phosphorus- and nitrogen-containing compounds, which contribute to the charring of the epoxy matrix and lead to a compact and intumescent char with highly carbonized aromatic networks. The element composition of the char residue after CCT is analyzed by XPS (see Table S4†). Both EP-0 and EP-4.0 contain C, O and N elements. Compared to EP-0, the P element is found in EP-4.0 with a content of 0.32 wt%, which agrees with the FT-IR results and further confirms that MBF-DOPO plays an important role in the condensed phase, which forms a phosphorus-rich char layer to inhibit the heat and gas transfer during combustion.

Thermal and mechanical properties

TGA is used for assessing the thermal stability of EP-0 and EP-4.0 under N_2 (Fig. 11) and air conditions (Fig. 12), the related data are shown in Table S5.† As shown in Fig. 11(a), in N_2 atmosphere, EP-0 and EP-4.0 have only one weight loss stage. Compared with EP-0, EP-4.0 has a slightly lower $T_{5\%}$ and maximum decomposition temperature ($T_{d,max}$) due to the less stable structures (P–O–C and P═O) from MBF-DOPO in EP-4.0. In Fig. 11(b), the maximum decomposition rate (R_{max}) of EP-4.0 is 27.4% min^{-1}, which is far lower than EP-0 (36.5% min^{-1}), suggesting that MBF-DOPO has a good inhibition effect on the thermal degradation of the epoxy matrix. The residual mass (at 700 °C) of EP-0 is 14.7%, whereas EP-4.0 is increased to 21.8%. The above results show that although the phosphorus-containing groups in the MBF-DOPO molecule decompose at a relatively low temperature at the early and middle stages of thermal degradation, the phosphorus-containing compounds formed by MBF-DOPO can inhibit the thermal degradation of epoxy matrix at high temperatures and promote the formation of a stable char residue, which leads to a high residual mass and flame retardancy. Under air atmosphere, as shown in Fig. 12, both EP-0 and EP-4.0 possess two degradation stages. The first degradation stage corresponds to the degradation of the epoxy matrix, the second degradation process corresponds to the further oxidation of char residues. Similarly, the introduction of MBF-DOPO helps to catalyze the degradation of the epoxy thermoset under air conditions, which leads to the decrease of EP-4.0 in $T_{5\%}$ and T_d. The early degradation of phosphorus-containing groups in MBF-DOPO is able to generate phosphorus-based acid, which is helpful to promote the char

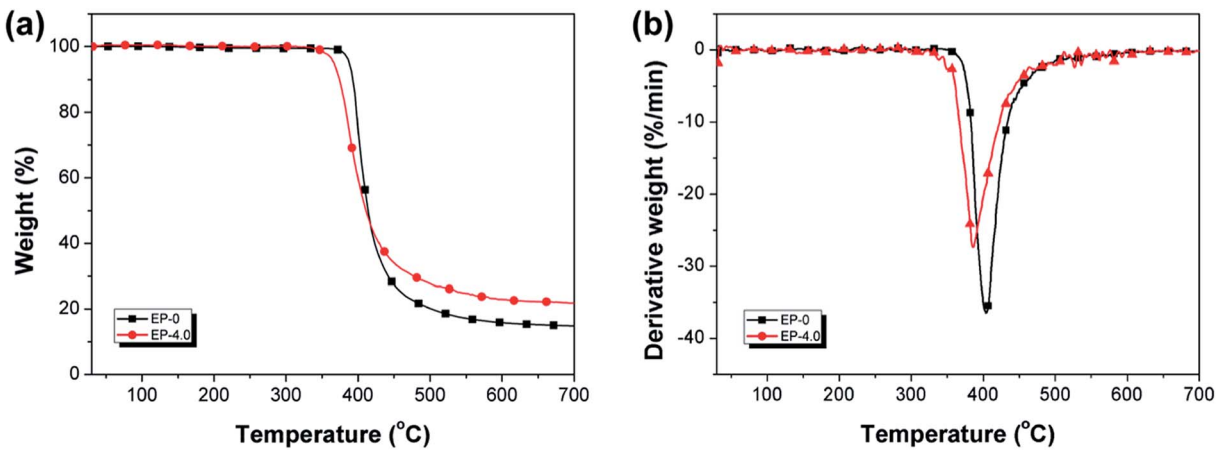

Fig. 11 (a) TGA and (b) DTG curves of EP-0 and EP-4.0 under N_2 conditions.

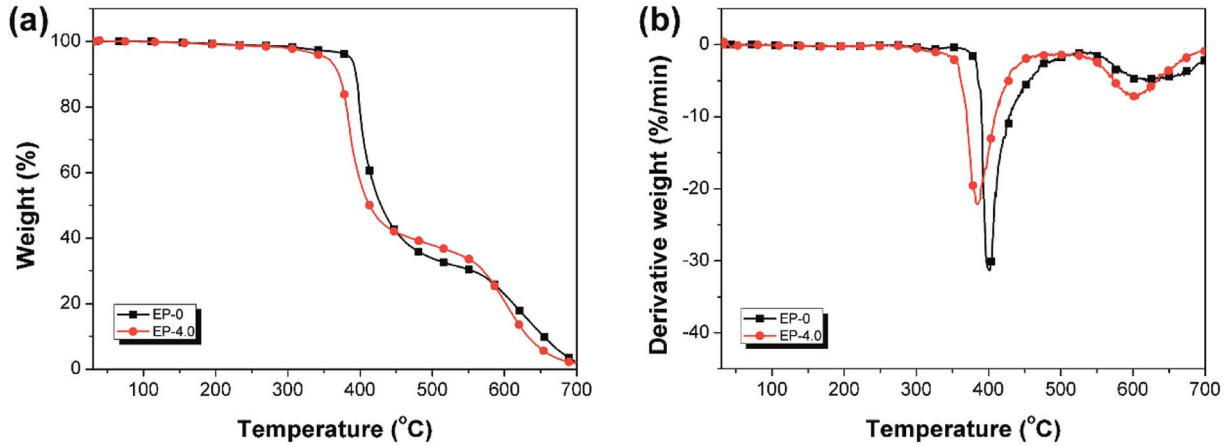

Fig. 12 (a) TGA and (b) DTG curves of EP-0 and EP-4.0 under air conditions.

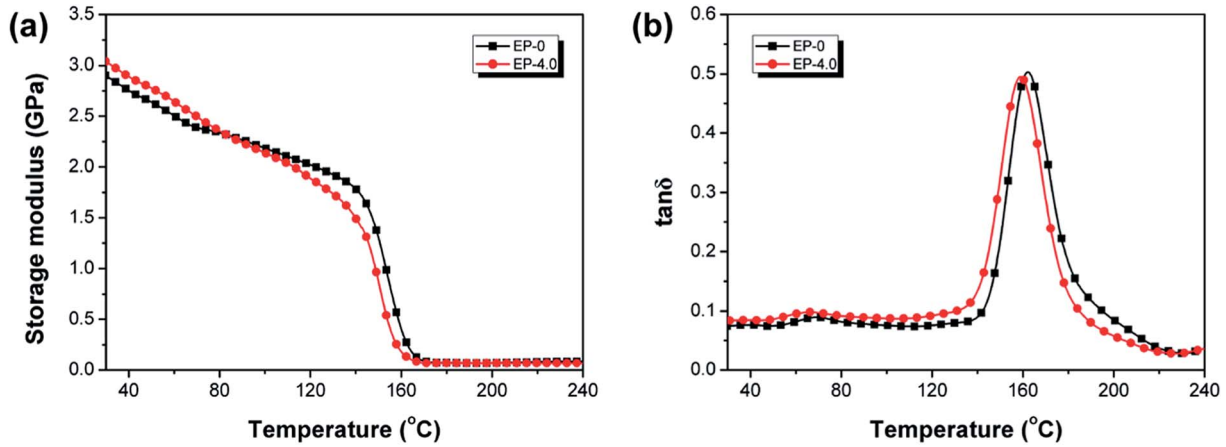

Fig. 13 (a) Storage modulus and (b) tan δ curves of EP-0 and EP-4.0.

forming of the epoxy matrix. As shown in Fig. 12(b), the R_{max} (21.8% min^{-1}) of EP-4.0 is also far lower than that (31.3% min^{-1}) of EP-0 under air atmosphere, suggesting that the phosphorus-based acid formed by MBF-DOPO can also decrease the degradation rate of the epoxy networks.

DMA is utilized for evaluating the thermomechanical performance of EP-0 and EP-4.0. The storage modulus (E') and loss factor (tan δ) curves are depicted in Fig. 13, the related data are shown in Table S6.† EP-4.0 possesses higher E' values (3.04 GPa) than EP-0 (2.89 GPa) at room temperature (30 °C), indicating that the rigid structures (phosphaphenanthrene and furan structure) in MBF-DOPO enhance the stiffness of the epoxy thermosets. In Fig. 13(b), EP-4.0 possesses a T_g (peak temperature in tan δ curve[26]) of 159.5 °C, which is only 2.7 °C lower than that of EP-0. Thus, EP-4.0 maintains the outstanding thermal stability of EP-0. The cross-link densities of EP-0 and EP-4.0 are calculated based on the literature,[27,28] as listed in Table S6.† The EP-4.0 shows a cross-link density of 4.99 × 10^3 mol m^{-3}, which is slightly lower than that of EP-0, suggesting that the introduction of MBF-DOPO leads to a slight decrease of the cross-link density of the epoxy resins.

The mechanical properties of EP-0 and EP-4.0 are evaluated (Table 3). Compared to EP-0, the tensile and flexural strengths of EP-4.0 are respectively decreased by 2.2% and 1.6%. These differences are mainly due to the lower cross-link density of EP-4.0. Meanwhile, the tensile and flexural moduli of EP-4.0 are respectively increased by 6.2% and 8.3%, which is mainly a result of the more rigid structures (*e.g.*, phosphaphenanthrene

Table 3 Tensile and flexural properties of EP-0 and EP-4.0

Samples	Tensile strength (MPa)	Tensile modulus (GPa)	Flexural strength (MPa)	Flexural modulus (GPa)
EP-0	71.8 ± 2.1	2.89 ± 0.11	105.5 ± 2.2	2.78 ± 0.12
EP-4.0	70.2 ± 1.9	3.07 ± 0.09	103.8 ± 3.1	3.01 ± 0.10

and furan structure) in MBF-DOPO.[29–31] In summary, the small content of MBF-DOPO has little impact on the mechanical performance of the EP-0 network.

Conclusions

Herein, a new furfural-based DOPO-containing flame retardant, namely 6,6′-(((methylenebis(4,1-phenylene))bis(azanediyl))bis(-furan-2-ylmethylene))bis(dibenzo[*c*,*e*][1,2]oxaphosphinine 6-oxide) (MBF-DOPO), was successfully prepared and utilized as a co-curing agent of 4,4′-diaminodiphenyl methane (DDM) for fire-safe epoxy thermosets. For the epoxy resin sample containing 4.0% MBF-DOPO, the limiting oxygen index (LOI) reached 32.9% (with a V-0 rating in the UL-94 test). Besides this, the mechanical and thermal performance of EP-4.0 were well maintained. Hence, MBF-DOPO has great potential for application in fire-safe epoxy thermosets. This work provides an effective and facile strategy to prepare a furfural-based DOPO-containing flame retardant.

Conflicts of interest

The authors declare that there are no conflicts of interest.

Acknowledgements

We gratefully acknowledge support from the National Natural Science Foundation of China (51573054), the Key Project in Science and Technology of Guangzhou (No. 201902010065), and the Opening Project of Key Laboratory of Polymer Processing Engineering (South China University of Technology), Ministry of Education, China (No. KFKT1702).

References

1 G. Tsilomelekis, M. J. Orella, Z. Lin, Z. Cheng, W. Zheng, V. Nikolakis and D. G. Vlachos, *Green Chem.*, 2016, **18**, 1983–1993.
2 L. Bao, L. Shi, H. Luo, L. Kong, S. Li, W. Wei and Y. Sun, *ChemSusChem*, 2017, **10**, 3040–3043.
3 D. Steinbach, A. Kruse and J. Sauer, *Biomass Convers. Biorefin.*, 2017, **7**, 247–274.
4 Y. Fan, D. Zhang, A. Zheng, Z. Zhao, H. Li and T. Yang, *Chem. Eng. J.*, 2019, **358**, 743–751.
5 N. Esmaeili, M. J. Zohuriaan-Mehr, S. Mohajeri, K. Kabiri and H. Bouhendi, *Eur. J. Wood Wood Prod.*, 2017, **75**, 71–80.
6 Z. J. Brentzel, K. J. Barnett, K. Huang, C. T. Maravelias, J. A. Dumesic and G. W. Huber, *ChemSusChem*, 2017, **10**, 1351–1355.
7 F. Zhou, Z. Guo, W. Wang, X. Lei, B. Zhang, H. Zhang and Q. Zhang, *Compos. Sci. Technol.*, 2018, **167**, 79–85.
8 F. Jeyranpour, G. Alahyarizadeh and A. Minuchehr, *Polymer*, 2016, **88**, 9–18.
9 F.-L. Jin, X. Li and S.-J. Park, *J. Ind. Eng. Chem.*, 2015, **29**, 1–11.
10 W.-Q. Xie and X.-S. Chai, *Polym. Test.*, 2017, **59**, 113–117.
11 S. Wang, S. Ma, C. Xu, Y. Liu, J. Dai, Z. Wang, X. Liu, J. Chen, X. Shen and J. Wei, *Macromolecules*, 2017, **50**, 1892–1901.
12 S. Yang, J. Wang, S. Huo, J. Wang and Y. Tang, *Polym. Degrad. Stab.*, 2016, **126**, 9–16.
13 Y. Chen, H. B. Zhang, Y. Yang, M. Wang, A. Cao and Z. Z. Yu, *Adv. Funct. Mater.*, 2016, **26**, 447–455.
14 L. Zhang, Y. Wang, Q. Liu and X. Cai, *J. Therm. Anal. Calorim.*, 2016, **123**, 1343–1350.
15 M.-J. Xu, G.-R. Xu, Y. Leng and B. Li, *Polym. Degrad. Stab.*, 2016, **123**, 105–114.
16 P. Wang and Z. Cai, *Polym. Degrad. Stab.*, 2017, **137**, 138–150.
17 L. Costes, F. Laoutid, S. Brohez and P. Dubois, *Mater. Sci. Eng., R*, 2017, **117**, 1–25.
18 X. Zhao, D. Xiao, J. P. Alonso and D.-Y. Wang, *Mater. Des.*, 2017, **114**, 623–632.
19 R. Ménard, C. Negrell, M. Fache, L. Ferry, R. Sonnier and G. David, *RSC Adv.*, 2015, **5**, 70856–70867.
20 C.-M. Lin, C.-H. Chen, C.-H. Lin and T.-Y. Juang, *Eur. Polym. J.*, 2018, **108**, 48–56.
21 W. Xu, A. Wirasaputra, S. Liu, Y. Yuan and J. Zhao, *Polym. Degrad. Stab.*, 2015, **122**, 44–51.
22 F. Ferdosian, Y. Zhang, Z. Yuan, M. Anderson and C. C. Xu, *Eur. Polym. J.*, 2016, **82**, 153–165.
23 Y. Wen, Z. Cheng, W. Li, Z. Li, D. Liao, X. Hu, N. Pan, D. Wang and T. R. Hull, *Polym. Degrad. Stab.*, 2018, **156**, 111–124.
24 C. Dong, A. Wirasaputra, Q. Luo, S. Liu, Y. Yuan, J. Zhao and Y. Fu, *Materials*, 2016, **9**, 1008.
25 T. Mariappan, Y. Zhou, J. Hao and C. A. Wilkie, *Eur. Polym. J.*, 2013, **49**, 3171–3180.
26 J. Michels, R. Widmann, C. Czaderski, R. Allahvirdizadeh and M. Motavalli, *Composites, Part B*, 2015, **77**, 484–493.
27 X. Xu, S. Ma, J. Wu, J. Yang, B. Wang, S. Wang, Q. Li, J. Feng, S. You and J. Zhu, *J. Mater. Chem. A*, 2019, **7**, 15420–15431.
28 R. Rahul and R. Kitey, *Composites, Part B*, 2016, **85**, 336–342.
29 R. Chatterjee, S. Bisoi, A. G. Kumar, V. Padmanabhan and S. Banerjee, *ACS Omega*, 2018, **3**, 13510–13523.
30 J.-T. Miao, L. Yuan, Q. Guan, G. Liang and A. Gu, *ACS Sustainable Chem. Eng.*, 2017, **5**, 7003–7011.
31 J. Deng, X. Liu, C. Li, Y. Jiang and J. Zhu, *RSC Adv.*, 2015, **5**, 15930–15939.